Excited-State Dynamics of Nitrated Push−Pull Molecules: The Importance of the Relative Energy of the Singlet and Triplet Manifolds

Elisa Collado-Fregoso, Jimena S. Zugazagoitia, Eddy F. Plaza-Medina, and Jorge Peon*

Instituto de Química, Universidad Nacional Autónoma de México, Circuito Exterior, Ciudad Universitaria, México, 04510, D.F., Mexico

Received: June 8, 2009; Revised Manuscript Received: September 14, 2009

We present a study of the dynamics following photoexcitation in the first electronic band of NO_2-*para*-substituted nitronaphthalenes. Our main goal was to determine the interplay between the nitro group, electron-donating substituents, and the solvent in defining the relative excited-state energies and their photoinduced pathways. We studied 4-nitro-1-naphthylamine and 1-methoxy-4-nitronaphthalene in solution samples through femtosecond fluorescence up-conversion and transient absorption techniques. In all solvents, both compounds have ultrafast fluorescence decays, showing that, similarly to the parent compound 1-nitronaphthalene, these molecules have highly efficient S_1 decay channels. The evolution of the transient absorption signals in the visible region reveals that for the methoxy-substituted compound, independently of solvent polarity, the photophysical pathways are the same as in 1-nitronaphthalene, namely, ultrafast intersystem crossing to an upper triplet state (receiver T_n state) followed by relaxation into the lowest energy phosphorescent triplet T_1. In contrast, for the amino-substituted nitronaphthalene, the excited-state evolution shows a strong solvent dependence: In nonpolar solvents, the same type of intersystem crossing through an upper receiver triplet state dictates the photochemistry. However, in methanol, where the first singlet excited state shows an important solvent-induced stabilization, we observed typical signals of the repopulation of the electronic ground state in the time scale of less than 1 ps followed by vibrational cooling within S_0. Excited-state calculations at the time-dependent density functional level with the PBE0 functional give an approximate characterization of the states involved and appear to correlate well with the experimental results as they show that the S_1 state of the amino compound is stabilized with respect to upper triplet states only in the polar solvent. These findings sustain and illustrate the recent view that the intersystem crossing channel so prevalent in nitroaromatic compounds is related to an energy coincidence between the $\pi-\pi^*$ first singlet excited state and upper triplet states with $n-\pi^*$ character. Our results indicate through direct observations that if the S_1 state is sufficiently stabilized, other rapid decay channels like internal conversion to the ground state will minimize the transfer of population to the triplet manifold.

Introduction

When a nitro group is directly bonded to an aromatic system, it drastically changes the photochemistry of the molecule. First, the $-NO_2$ nonbonding orbitals greatly increase the spin−orbit coupling of the spectroscopic singlet states with the triplet manifold.[1−10] This feature makes most nitrated polycyclic aromatics virtually nonfluorescent but highly phosphorescent, and also determines that all of the secondary bimolecular photochemistry, such as, for example, electron and proton transfer, occurs from the lowest energy triplet state.[11−13] Another influence of this group is that, acting as an electron-withdrawing substituent, it allows an extension of the ring aromaticity, which stabilizes electronically excited states with transition dipole moments aligned in the direction of the $-NO_2$ group, also giving these states a charge-transfer character. Such effect makes nitroaromatics have their first UV−vis absorption bands at significantly longer wavelengths in comparison with the unsubstituted aromatics (1-nitronaphthalene vs naphthalene, 9-nitroanthracene vs anthracene, 1-nitropyrene vs pyrene, etc.).[14−18] Related to their environmental photochemistry, it has been established that nitrated polycyclic aromatic hydrocarbons (NPAHs) are considerably more photoreactive than the respective unsubstituted polyaromatics.[19−23] Although several channels may contribute to NPAH's environmental and solution photochemistry, one of the most important ones is a direct rearrangement of the $-NO_2$ group leading to the formation of the respective aryloxy radical (Ar−O•) and photodetachment of nitric oxide (NO•).[24] This channel has been observed in nitrobenzene, 9-nitroanthracene, some 10-substituted 9-nitroanthracenes, 1-nitropyrene, and 6-nitrobenzo[*a*]pyrene,[16,25−28] but not in nitronaphthalenes like the ones of the present study, where only secondary bimolecular photochemistry of the T_1 state has been observed.[11−14,29]

The efficient photogeneration of highly reactive species, like the triplet states as well as the Ar−O• and NO• fragments, has made nitroaromatic compounds interesting candidates for photodynamic therapies,[25,30,31] and useful initiators in photopolymerization schemes.[32,33] These potential applications and their remarkable photochemistry make it important to understand the dynamics of their electronically excited states through experiments which resolve the system's evolution immediately after the photon absorption event. As mentioned previously, the most determinant feature of nitroaromatic's photochemistry is their highly efficient intersystem crossing (this includes the case of the NO• releasing compounds where the photodissociation channel occurs with a low yield in parallel with the principal

* Corresponding author. E-mail: jpeon@servidor.unam.mx.

10.1021/jp905379y CCC: $40.75
Published on Web 10/19/2009

T_1 formation channel[16,28]). From the early studies of Hamanoue and Mikula,[4,14] it has been suggested that the efficient triplet formation in these molecules is related to the presence of upper triplet states, which exist at energies similar to that of the S_1 state. These "receiver" triplet states have been considered to have electronic configurations, which involve the excitation from the nonbonding orbitals (T_n states with n−π* character at higher energies than the phosphorescent triplet T_1 of π−π* character,[6,7,14] consistently with selection rules for transitions between manifolds[34]). Actually, recent calculations at the time-dependent density functional theory (TD-DFT) level do predict the existence of such type of upper triplet states in molecules like 1-nitronaphthalene and 1-nitropyrene, where it has been determined that it is probably the third triplet state T_3 that most contributes to the manifold crossing as it has at least a partial n−π* character and lies at a slightly lower energy than the S_1 state in solution.[15,17]

Our group recently completed a series of femtosecond fluorescence and transient absorption studies, which indicate that the singlet−triplet crossing in polycyclic nitrated compounds can occur in an ultrafast time scale, giving rise to intermediary states within 100 fs. These states were assigned as those suggested by Hamanoue and Mikula (triplet, n−π* states) and were observed directly for the first time in 1-nitronaphthalene.[35] The relaxation of the system into the lowest energy phosphorescent triplet state was observed to be completed in a slower time scale of more than 10 ps due to internal conversion and vibrational cooling within the triplet manifold. In these latter steps, the system is required to release about 1 eV of energy to the medium.

In this contribution, we further explore the details of the manifold crossing in nitroaromatics. Specifically, we inquire whether the typical photophysical pathway can be altered by stabilization of the S_1 state. We addressed this question through direct measurements of the excited-state evolution of 1-nitronaphthalenes with an additional electron-donating substituent at the NO_2-*para* position. We have observed how with the additional groups, variations in the polarity of the solvent environment can limit the intersystem crossing channel. In particular, we made comparisons between two substituted nitronaphthalenes: 4-nitro-1-naphthylamine (NNA) and 1-methoxy-4-nitronaphthalene (MNN). Next, we make a brief review of the relevant aspects of these two molecules.

For MNN, it has been established that all of the photochemistry is due to secondary bimolecular reactions of the triplet state, including substitution and electron transfer, indicating that rapid intersystem crossing from the first excited singlet state is the main primary photoinduced pathway. The absorption from the (phosphorescent) triplet state of this molecule has also been identified in flash photolysis experiments.[12,13] While the fluorescence from the compound is undetectable by steady-state methods, implying a quantum yield (ϕ_{fluor}) of less than 10^{-3},[13] the quantum yields for singlet oxygen formation in MNN in O_2-saturated benzene and acetonitrile solutions are 0.4 and 0.36, respectively, which correspond to an approximate lower limit of the triplet quantum yield.[13]

NNA is almost nonfluorescent ($\phi_{fluor} \approx 10^{-5}$ in a 77 K matrix,[32] with fluorescence centered at 462 nm). Nanosecond flash photolysis experiments by Capellos et al. also have detected the $T_n \leftarrow T_1$ transient absorbance of this compound in benzene and polymethyl methacrylate (PMMA) in solution at room temperature and at −150 °C. However, when the photolysis was made in methanol solution, in the time scale of nanoseconds and microseconds, no transient species was detected.[29] In this contribution, we include the first detailed description of the femtosecond and picosecond dynamics of MNN and NNA, which clarifies the early photodynamics of both compounds, including the participation of intermediary states as well as the solvent dependence in NNA.

To get an idea of the orbitals involved in the different electronic states that participate in the studied phenomena, we include TD-DFT calculations on MNN and NNA considering solvent effects through the polarizable continuum model (PCM). This level of calculations is a cost-efficient way to estimate the character of the transitions (charge transfer, π−π* vs n−π*) and to determine if the solvent affects in the same way the different states that may participate in the intersystem crossing channel and overall photodynamics.

Methodology

Experimental Methods. High-performance liquid chromatography grade methanol and cyclohexane, and anhydrous benzene were obtained from Aldrich. MNN and NNA were acquired from Aldrich and recrystallized from methanol and ethanol, respectively, before used. Steady-state absorption spectra of the solutions were taken in a Cary-50 spectrophotometer (Varian) in 1 mm quartz cells. Our setup for femtosecond fluorescence up-conversion has been described in detail previously.[36] A 100 fs pulse train was generated in a standard 100 MHz Ti:Sapphire oscillator, and the excitation pulses were generated by frequency doubling in a 0.5 mm β-BBO crystal. The polarization of the second harmonic beam (pulse energy at the sample: 0.2 nJ) was rotated to the magic angle with a half wave plate before it was focused into a 1 mm path length flow cell containing the samples. The fluorescence was refocused with the aid of a pair of parabolic mirrors, and the emission intensity was time-resolved by sum frequency mixing it with a vertically polarized and temporally delayed pulse from the remaining fundamental in another 0.5 mm β-BBO crystal. The sum-frequency mixing signal with horizontal polarization was refocused into a double monochromator and detected with a photomultiplier tube connected to a lock-in amplifier referenced to a 200 Hz optical chopper in the path of the pump beam. The instrument response function for our up-conversion measurements was determined for the different experimental conditions (sample and excitation wavelengths) through cross-correlation measurements between the gate pulses and the Raman scattering of the second harmonic pulses by the solvents. For all experiments, back to back solvent-only scans were taken to ensure that the rapid signals we observed for the solutions were not present in the solvent-only traces.

The setup for our transient absorption measurement has been described elsewhere.[35] It is based on a 1 kHz pulse train from a regeneratively amplified femtosecond laser (~150 fs, 0.5 mJ/pulse). About 1% of the energy of the main beam was used to generate a white light continuum in a 1 mm z-cut Sapphire plate, and the rest was used to generate the pump beam by passing it through a frequency doubling 0.5 mm β-BBO crystal. The second harmonic pulse train was then separated from the remaining fundamental with a dichroic mirror, and its polarization was adjusted to the magic angle with respect to the polarization of the probe pulse (horizontal) and focused approximately 6 cm after the sample for a beam diameter of 0.8 mm at the sample, a diameter at least 4 times larger than the probe beam spot size as measured by the knife-edge technique. The pulse energy for most experiments was 50 μJ except for the samples in benzene where the pulse energy needed to be reduced to less than 10 μJ to avoid two-photon excitation of

the solvent. After traversing a 1 mm flow cell (MNN and NNA/benzene measurements), or a 0.45 mm free-flowing jet (NNA/methanol) with the solution sample, the probe beam was focused into a 10 cm focal-length monochromator and detected with a photodiode connected to a lock-in amplifier referenced to an optical chopper operating at the third subharmonic of the 1 kHz amplified pulse train. With this, the pump pulse train was synchronized and phase-adjusted with the white light train so that the sample received only one of every three second harmonic pulses. The instrumental response function for each probe wavelength, sample (jet or flow cell), and alignment condition was estimated from the $t = 0$ signal from the solvent alone due to cross-phase modulation between the pump and the continuum pulse and is indicated in the respective tables of the results section. Transient absorption spectra at long delay times were taken by scanning the detection wavelength of the monochromator while detecting the transient absorption signal. These spectra were taken to identify transient species that persist at long times ($t > 100$ ps), and to scale single-wavelength time traces. Because there is no spectral evolution at such long times, correction for the dispersion of the different probe wavelengths was unnecessary.[37] For the NNA/methanol experiments, where the signals have fast decays, short time scans (up to 5 ps) at all of the different wavelengths were taken on the same day with the same exact experimental condition to ensure that the relative ΔAbs measurements were correct and to scale the long single-wavelength time scans taken on different days. For all experiments, the integrity of the sample was verified by UV−vis spectroscopy throughout the data acquisition and replaced frequently to avoid the appearance of photoproducts. All experiments were performed at room temperature (20 ± 1 °C) under aerated conditions.

Computational Methods. Properties of the low-lying excited states of MNN and NNA were calculated with the TD-DFT method using the 6-311++G(d,p) basis set and the PBE0 hybrid functional. We have chosen this particular functional because it has been shown that, given a large enough base, it gives an adequate description of two ring systems (naphthalenic).[15,38,39] Because solvent effects play a central role in our experiments, we considered the effects for benzene and methanol solutions through the Polarizable Continuum Model (PCM, nonequilibrium solutions for the TD-DFT calculations). The vertical transition energies correspond to the ground-state-optimized geometry with the same basis set, functional, and solvent model. Stationary points without imaginary frequencies were verified, keeping the default thresholds for self-consistency and optimization. For all calculations, the Gaussian 03 program was used.[40]

Results and Discussion

Steady-State Spectroscopy. Our study focuses on the dynamics following excitation in the first electronic band of MNN and NNA. Figures 1 and 2, respectively, show the steady-state absorption spectra in the region of the first electronic transition for both compounds in methanol and benzene. As can be seen, these molecules have a symmetric and well-defined first electronic band in the near UV that are similar in both shape and oscillator strength to the first electronic transition seen in 1-nitronaphthalene. In this parent compound, the UV−vis spectra and previous TD-DFT and CNDO−CI calculations indicate that the first band is associated with a nearly short axis polarized, $\pi-\pi^*$ type transition to the first excited singlet state. This state resembles the $^1B_{2u}$ state of naphthalene in the oscillator strength of the transition, the direction of the transition dipole moment, and the types of orbitals involved.[15] Similarly to other

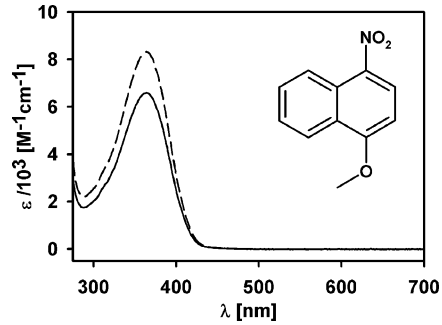

Figure 1. Molecular structure of 1-methoxy-4-nitronaphthalene and steady-state absorption spectra in benzene (− − −) and methanol (−).

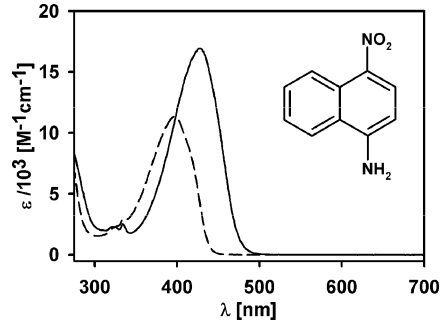

Figure 2. Molecular structure of 4-nitro-1-naphthylamine and steady-state absorption spectra in benzene (− − −) and methanol (−).

1-substituted naphthalenes, this kind of transition becomes highly stabilized due to an extension of the conjugation along the short axis of the molecule thanks to the electron-withdrawing character of the nitro group at the α position. The systems of our study also show this characteristic first band except that the π-electron-donating groups at the NO_2-*para* position further stabilize the first transition due to an increased charge-transfer character from the "push−pull" effect. This first band has its maximum at 364 nm for MNN in both solvents and at 396 and 427 nm for NNA in benzene and methanol, respectively. In both compounds, the band remains a mid intensity transition with absorption coefficients at the maximum between 6×10^3 and 17×10^3 M^{-1} cm^{-1}. From Figure 2, it is clear that the amino-substituted compound allows for a marked solvatochromic effect in going from benzene to methanol, where the transition energy is lowered from 3.13 to only 2.90 eV. Such an important change in the steady-state spectra can be related to an intramolecular charge-transfer process that takes place upon excitation, as it happens with the similar compound *para*-nitroaniline. For this last compound, it has been established that the charge transfer from the amino to the nitro group leads to a vast change on the dipole moment upon excitation, which in turn causes the compound's molecule to be very sensitive to the nature and polarity of the solvent.[41,42] On the other hand, for MNN, the first transition is practically insensitive to the solvent polarity (∼3.40 eV). Because the objective of the present study was to observe differences in the photophysics associated with changes in the relative energy of the first singlet excited state, the different behavior of the first transition of NNA in going from the nonpolar to the polar solvent will serve to suggest the importance of particular energy coincidences between the S_1 state and the triplet manifold.

Excited-State Calculations. To obtain more insights into the nature of the first electronic transitions, we made a series of excited-state calculations at the TD-DFT level accounting for the solvent effects through the PCM model. The calculated

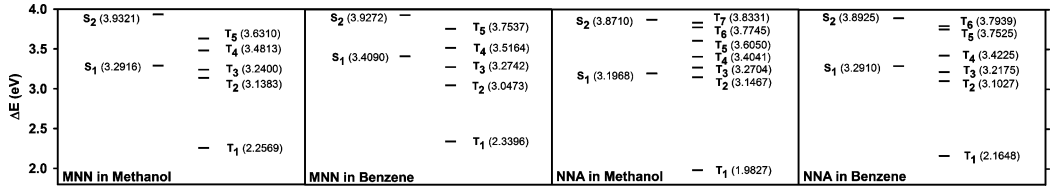

Figure 3. Excited-state energy diagrams for 1-methoxy-4-nitronaphthalene (MNN) and 4-nitro-1-naphthylamine (NNA) at the TD-DFT/6-311++G(d,p) level of theory with the PBE0 functional and the PCM model for solvation effects in benzene and methanol. Calculations correspond to the DFT ground-state-optimized geometry with the same functional, basis set, and solvent model.

energies of the low-lying excited states of MNN and NNA at the ground-state-optimized geometries are shown in Figure 3. Both in MNN and in NNA, the nitro group is twisted out of the naphthlalenic plane by an angle between 15.95° (NNA/methanol) and 26.22° (MNN/methanol) due to a balance between the steric hindrance with the hydrogen at the peri position and the NO_2 conjugation with the rings. In MNN, the methoxy substituent in both solvents is aligned practically into nearly full coplanarity to increase the π interaction with the ring system (considers the plane defined by the $C_{aromatic}-O-C_{methyl}$ bonds). On the other hand, the NH_2 geometry in NNA shows differences depending on the solvent. In benzene, there is a clear wagging of the amino hydrogen atoms, whereby the N−H bonds define dihedral angles of 19.65° and 11.55° with respect to the naphthalenic plane (both hydrogens on the same side of this plane). On the other hand, in methanol, both N−H bonds lie practically in the same plane of the ring system (dihedral angles of less than 4°, and maintaining all of the NH_2 atoms nearly in the same plane). Optimized coordinates and depictions of these structures are included in the Supporting Information. The much better coplanarity of the NH_2 atoms for NNA in methanol indicates a larger overall conjugation in this system, which is in turn related to the solvatochromism observed for the first transition in this solvent.

The TD-DFT-calculated first electronic transitions show a typical deviation from the experimental result for this method of between 0.11 eV (MNN in benzene) and 0.297 eV (NNA in methanol). The first singlet−singlet electronic transition for both molecules in both solvents has a HOMO−LUMO character with a larger than 0.6 TD-DFT coefficient (see Supporting Information for geometries, transition coefficients, and orbital depictions). Diagrams of the Kohn−Sham orbitals indicate that the HOMO orbitals have the same distribution of nodal planes as 1-nitronaphthalene's HOMO and naphthalene's a_u frontier orbital in the rings. Similarly, the LUMO orbitals have the same nodal plane distribution as 1-nitronaphthalene's LUMO and show large contributions from the basis functions at the atoms of the nitro group. Such inspection allows a characterization within this level of theory of the first optical transition as dominated by a $\pi-\pi^*$ character, for both MNN and NNA. The transition dipole moment from the ground state is in fact nearly parallel with the short molecular axis (from 3.0° for MNN/methanol to 1.3° for NNA/methanol with respect to the inner naphthalenic C=C bond). It should be mentioned that the lowest energy triplet state is again dominated by the same $\pi-\pi^*$ transition (HOMO−LUMO, coefficient >0.7), similarly to what has been pointed out for 1-nitronaphthalene on the basis of theoretical[14,15] and experimental results.[6,7] Relevant for the present discussion, the TD-DFT calculations also indicate that for MNN in both solvents and for NNA in benzene, the S_1 state lies slightly above the two upper triplet states T_2 and T_3. This same feature has been observed and discussed previously in more detail for 1-nitronaphthalene.[15] Both of these triplet states have contributions from multiple single-electron excitations, which include, among

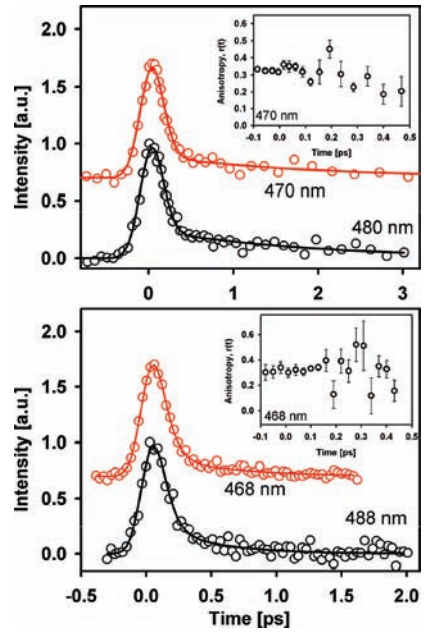

Figure 4. Fluorescence up-conversion results for 1-methoxy-4-nitronaphthalene in benzene (top) and methanol (bottom). Solid lines indicate fits for biexponential decays convoluted with the instrument response function. Insets show anisotropy results. For clarity, traces at different wavelengths have been shifted in the ordinate axis.

others, the HOMO-2−LUMO and HOMO-3−LUMO transitions. Visual inspection of the orbitals involved shows that such excitations give these two upper triplet states at least a partial $n-\pi^*$ character. Interestingly, for the NNA system, the TD-DFT results indicate that the S_1 state is stabilized below the T_3 state in methanol (see Figure 3).

Femtosecond-Resolved Fluorescence Measurements. Compounds with negligible fluorescence quantum yields can have significant fluorescence signals when the spontaneous emission is resolved within the first few hundreds of femtoseconds following photoexcitation.[43,44] Characteristic examples of this are polycyclic nitroaromatic compounds that had previously been termed nonfluorescent, but where up-conversion experiments have been able to follow the subpicosecond decay of their S_1 state.[36] Following emission signals from these states is of great value in photophysical studies because this allows a much clearer interpretation of the results from other experiments like transient absorption where several species will contribute to the signals. Figures 4 and 5 show representative results of femtosecond up-conversion measurements on MNN and NNA. For both compounds, it was possible for the first time to make direct observations of their fluorescence decays.

First, for MNN, the sum-frequency signals in both methanol and benzene decay as biexponential functions. The characteristic times and coefficients for representative traces are included in the first two rows of Table 1. Here, a sub-100 fs component accounts for more than 90% of the signal's amplitude, and the

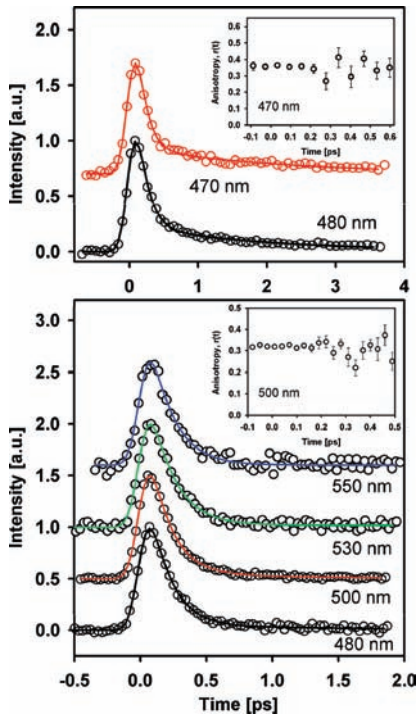

Figure 5. Fluorescence up-conversion results for 4-nitro-1-naphthylamine in benzene (top) and methanol (bottom). Solid lines indicate fits for biexponential decays convoluted with the instrument response function. Insets show anisotropy results. For clarity, traces at different wavelengths have been shifted in the ordinate axis.

TABLE 1: Curve-Fitting Parameters for Selected Fluorescence Up-Conversion Traces of 1-Methoxy-4-nitronaphthalene (MNN) and 4-Nitro-1-naphthylamine (NNA) in Benzene and Methanol[a]

compound	solvent	λ_{exc} [nm]	λ_{fluo} [nm]	a_1	τ_1 [ps]	a_2	τ_2 [ps]
MNN	methanol[b,f]	396	468	0.94	0.07	0.06	0.52
MNN	benzene[b,c,g]	389	470	0.96	≤0.07	0.04	1.84
NNA	methanol[d,f]	395	498	0.96	0.17	0.04	1.79
NNA	methanol[d,e,h]	415	500	0.95	0.15	0.05	0.78
NNA	methanol[d,h]	415	550	1	0.17		
NNA	benzene[d,i]	410	490	0.96	0.13	0.10	2.13

[a] Data are described by single- or double-exponential functions, $I(t) = \sum_i a_i \cdot \exp(-t/\tau_i)$, convoluted with the instrument response function. The sum of parameters a_1 and a_2 is normalized to one. The estimated errors in the time constants are shown in the following footnotes. [b] Between 9% and 17%. [c] τ_1 value is below the instrumental resolution. [d] Between 3% and 16%. [e] τ_2 has an estimated error of 20%. Instrument response functions are shown in the following footnotes. [f] 190 fs. [g] 320 fs. [h] 150 fs. [i] 230 fs.

rest is associated with a second exponential term with time constants of about 0.5 ps for MNN in methanol and 1.8 ps for MNN in benzene. Since for this compound it has been seen that the main photoinduced channel is the formation of the first triplet state,[12,13] these measurements reflect the ultrafast wave packet evolution in the S_1 potential energy surface and loss of population due to radiationless transitions (see below, transient absorption results and kinetic model). The existence of a double-exponential decay appears to be somewhat common in nitrated polyaromatics because the same has been observed in other systems such as 9-nitroanthracene, 1-nitropyrene, 6-nitrochrysene, and 3-nitrofluoranthene.[17,36]

The insets in Figure 4 show fluorescence anisotropy determinations for MNN, which were calculated directly according to $r(t) = (I_{||} - I_{\perp})/(I_{||} + 2 \cdot I_{\perp})$ from traces resolving the parallel ($I_{||}$) and perpendicular ($I_{\perp}$) components of the spontaneous emission with respect to the excitation polarization axis. The $r(t)$ measurements were made to distinguish if during the first exponential decay there was a significant change in the transition dipole direction, which would speak about a possible change in the electronic state responsible for the emission. The anisotropy measurements show an initial value consistent with nearly parallel absorption and emission transitions (~0.3). Despite the double-exponential form of the fluorescence intensity, the $r(t)$ trace does not show any sharp changes in time scale of the decay of the ~70 fs component, but only a slow decay consistent with the rotational relaxation of the excited-state population, which is not completed before the emission has fully decayed.

In the same way as MNN, for the amino-substituted compound, the fluorescence can only be detected in the femtosecond and few picoseconds time scale. For the NNA/methanol system, the fluorescence signal obeys a single- or double-exponential decay depending on the detection wavelength, with time constants below 200 fs for the fast (or only) component, and between ~0.8 and ~1.8 ps for the slower component. The results are summarized in the last rows of Table 1. Changing the excitation wavelength from 395 to 415 nm has negligible effects in the decays. For the NNA/benzene system, again double-exponential decays are seen where the fast time constant is around 130 fs and the slower one is between ~1.8 and ~2.1 ps. Once more, for this compound, the anisotropy measurements (insets in Figure 5) indicate that there are no changes in the direction of the transition dipole moment as the fast exponential term decays, leaving the smaller contribution of the longer component. A complete set of tables with fluorescence up-conversion fitting parameters for both MNN and NNA can be found in the Supporting Information.

Following the interpretation in our previous studies of NPAHs,[36] the biexponential decay of S_1 is associated with a kind of local relaxation of the excited-state from the original geometry accessed by vertical transition. Because the anisotropy of the emission is maintained throughout the biexponential decay, and considering the time scales, these signals are most likely related to wave packet like motion of the nitro group within the same singlet potential energy surface (possibly, also including some inertial motion of the solvent molecules). This interpretation is also consistent with recent experimental and computational results on 1-nitropyrene by Crespo-Hernández et al.,[17] where the equilibrium S_1 geometry was determined to have the $-NO_2$ group nearly in the same plane of the polyaromatic system, while in the vertically accessed geometry from the electronic ground state, the $-NO_2$ unit has a torsion angle of approximately 27.46° (due to a balance between the steric hindrance with the peri-hydrogen and the π interactions also discussed herein for MNN and NNA). Similarly, for molecules like anthracene with a 9-carboxy or 9-carbomethoxy substitution (π-isoelectronic to 9-nitroanthracene), high resolution excitation and fluorescence spectra in the gas phase have shown that there is a large torsional angle change for the substituent in going from the ground state to the more planar first electronically excited state.[45,46]

A general kinetic scheme to account for the relaxation, which allows for simultaneous depletion processes, considers that the initially formed state S_1^{ini} responsible for the sub-200 fs fluorescence has nonradiative disappearance channels associated with the rate constant k_{depl}^{ini} and that, in parallel, this species undergoes the conformation change associated with k_{rel}^{ini} to a relaxed form S_1^{rel}, which has slower intrinsic depletion kinetics

SCHEME 1: General Kinetic Scheme of Primary Photoprocesses in Nitroaromatic Compounds with Biexponential Emission Decay

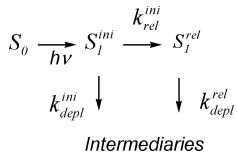

associated with the rate constant $k_{\mathrm{depl}}^{\mathrm{rel}}$ (and therefore, a longer second time constant τ_2 is measured, see below). These processes are summarized in Scheme 1. The solution of this kinetic scheme using standard techniques similar to the ones used for consecutive unimolecular reactions gives the populations of the two sequential forms of S_1 according to eqs 1 and 2. Considering that for the spectral region of our experiments emission from both forms is detected, the total signal evolution has the form of a biexponential function with time constants assigned as follows: $\tau_1 = (k_{\mathrm{depl}}^{\mathrm{ini}} + k_{\mathrm{rel}}^{\mathrm{ini}})^{-1}$ and $\tau_2 = (k_{\mathrm{depl}}^{\mathrm{rel}})^{-1}$. The intermediaries that result from the "depletion" channels of S_1^{ini} and S_1^{rel} will be identified from the transient absorption results.

$$S_1^{\mathrm{ini}}(t) = S_1^{\mathrm{ini}}(t_0)e^{-(k_{\mathrm{depl}}^{\mathrm{ini}}+k_{\mathrm{rel}}^{\mathrm{ini}})t} \quad (1)$$

$$S_1^{\mathrm{rel}}(t) = \frac{S_1^{\mathrm{ini}}(t_0)k_{\mathrm{rel}}^{\mathrm{ini}}}{k_{\mathrm{depl}}^{\mathrm{rel}} - k_{\mathrm{depl}}^{\mathrm{ini}} - k_{\mathrm{rel}}^{\mathrm{ini}}}(e^{-(k_{\mathrm{depl}}^{\mathrm{ini}}+k_{\mathrm{rel}}^{\mathrm{ini}})t} - e^{-k_{\mathrm{depl}}^{\mathrm{rel}}\cdot t}) \quad (2)$$

In summary, both MNN and NNA have biexponential decaying fluorescence signals where the majority of the signal (at least 89%) decays with a time constant of less than 200 fs, leaving a small contribution from a relaxed singlet geometry (S_1^{rel}) with a somewhat longer lifetime (subpicoseconds to less than 2 ps). As will be shown from the transient absorption measurements, it appears that, although the decay of the originally excited singlet is similar for all systems, the transfer of population to other states is actually different for NNA in methanol than for the other cases.

Transient Absorption Measurements. Figure 6 shows a summary of the transient absorption experiments of MNN in methanol solution. We will focus more on the details of the absorbance evolution for MNN in this solvent because the results in the nonpolar solvent are practically the same. The transient absorption traces were adjusted to either double- or triple-exponential functions, which account for increases (negative amplitude exponentials) or decaying terms. Because these traces were taken only at a limited number of wavelengths, for MNN the best-fit parameters were obtained through global fitting to joined time constants and allowing the coefficients to vary freely. The time constants obtained with this procedure correspond to 0.3, 2.7, and 9.8 ps, and the coefficients are included in the Supporting Information. Figure 7 shows a detail of the early times at 460 nm from where it can be seen that the 0.3 ps component is a well-defined rising component clearly differentiated from the $t = 0$ solvent spike present in these conditions. For all wavelengths, a long-lived ($\tau \gg 3$ ns) species is persistent after the early spectral evolution and is represented by the constant term in the fitting functions. The transient spectrum acquired at 150 ps is presented in Figure 6. From comparisons with previously published spectra,[12,13] this long-lived species

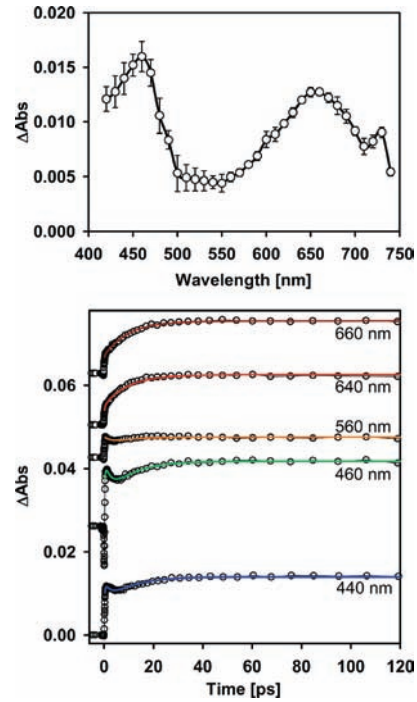

Figure 6. Transient spectrum acquired at 150 ps (top), and single-wavelength transient absorption traces (bottom) for 1-methoxy-4-nitronaphthalene in methanol. Solid lines correspond to fits to multi-exponential functions plus a constant term. These experiments show a $t = 0$ modulation due to the solvent and the flow-cell. Fits only include the time range where this modulation is absent. For clarity, single-wavelength transients have been shifted in the ordinate axis.

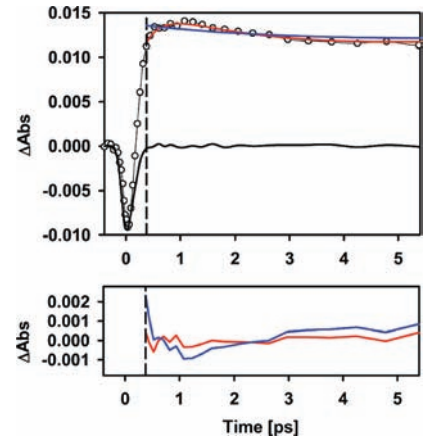

Figure 7. Top: Short time detail of the transient absorption experiment for 1-methoxy-4-nitronaphthalene in methanol at 460 nm. The solid blue line and the solid red line show, respectively, fits to double- or triple-exponential decays plus a constant term (see text). The solid black line is from an experiment with the solvent only. The vertical discontinuous line indicates the start of the time range for the fits where the solvent signal has fully returned to the baseline. Bottom: Residuals from the fits with double (blue line) and triple (red line) exponentials.

is identified as the phosphorescent triplet state of MNN, which was observed in experiments with nanosecond and microsecond resolution.

Because the long-lived species is fully recognized as T_1, the dynamics in the femtosecond and few picoseconds time scale are due to the formation of this state from other intermediaries. Since for the MNN/methanol system the fluorescent state decays with characteristic times of ~0.07 and 0.5 ps, the shortest time constant in the transient absorption evolution of 0.3 ps should

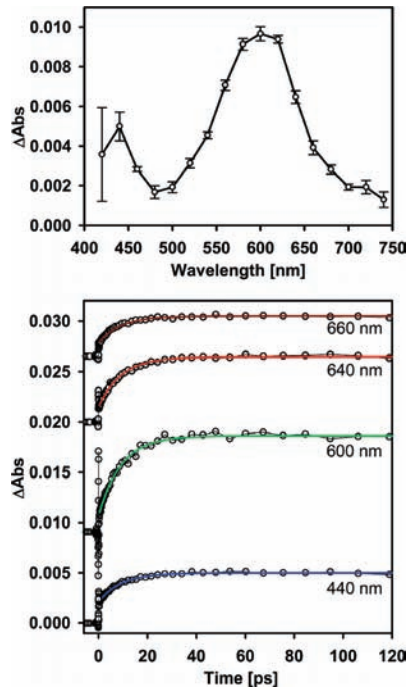

Figure 8. Transient spectrum acquired at 150 ps (top), and single-wavelength transient absorption traces (bottom) for 1-methoxy-4-nitronaphthalene in cyclohexane. Solid lines correspond to fits to an exponential rise to a constant level. These experiments show a $t = 0$ modulation due to the solvent and the flow-cell. For this system, the fits only include the time range where this modulation is absent. For clarity, single-wavelength transients have been shifted in the ordinate axis.

be assigned to the evolution of population from the singlet manifold. Because of the inferior time resolution of our transient absorption experiments, the 0.3 ps term represents a kind of average lifetime of the state resolved in the fluorescence experiments. As this term has negative amplitude, it indicates the accumulation of signal due to the intermediary state formed from S_1. In accordance with El-Sayed's rules and the dynamics observed in the parent compound 1-nitronaphthalene, the decay of the S_1 state is considered to be due to the coupling with an upper triplet state, which has contributions from n$-\pi^*$ configurations. For MNN/methanol, the formation of this "receiver" triplet state is observed predominantly between 440 and 460 nm where the 0.3 ps component has larger amplitudes. The triplet$-$triplet internal conversion and vibrational relaxation associated with the formation of the lowest energy phosphorescent triplet state of MNN are assigned to the other time constants of 2.7 and 9.8 ps, in correspondence with what was observed previously for 1-nitronaphthalene.[35] The main feature of these dynamics is a large increase of the transient absorbance in the visible region due to the accumulation of the fully relaxed T_1 state, which has a broad band centered at 660 nm and a peak at 460 nm (Figure 6), a transient spectrum quite similar to that of 1-nitronaphthalene's phosphorescent state.[12,13]

In Figure 8, we show the transient absorption spectrum for the case of MNN in cyclohexane measured at 150 ps. Again, at this time, the only species observed is the fully relaxed phosphorescent state. In this solvent, our experiments have a poorer time resolution due to the presence of signals from cross-phase modulation. Because of this effect, only the larger amplitude signal rise from the relaxation into T_1 is resolved and shown in Figure 8. The respective time constant was determined to be 9.09 ps through global fitting procedures, and the wavelength-dependent coefficients are included in the Supporting Information. We have also included in the Supporting Information representative single-wavelength transients of MNN in benzene with their respective fitting parameters, to sustain the fact that in both nonpolar solvents the excited-state dynamics of MNN follow the same trend.

SCHEME 2: General Deactivation Processes of the First Excited Singlet State in the Studied Nitroaromatic Compounds[a]

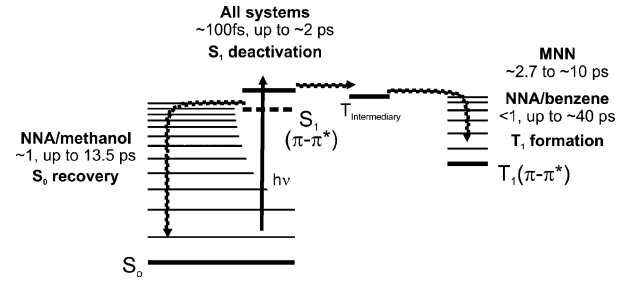

[a] The relative energies between the S_1 and $T_{intermediary}$ states dictate the predominant deactivation process in the studied nitroaromatic compounds: Because for 4-nitro-1-naphthylamine (NNA) in benzene and 1-methoxy-4-nitronaphthalene (MNN) S_1 and $T_{intermediary}$ are nearly isoenergetic (the S_1 state represented by the solid line), the system deactivates mainly by intersystem crossing toward the final formation of the fully relaxed T_1. On the other hand, for NNA in methanol the S_1 state is stabilized with respect to the intermediary triplet (the S_1 state represented by the dashed line), making the crossing between manifolds difficult to occur and leading the system to deactivate mainly by internal conversion to the S_0 state.

The results presented here for MNN in polar and nonpolar solvents resolve for the first time the earliest part of its photodynamics including the formation of an intermediary state (~0.3 ps, well resolved in methanol) and the consecutive relaxation steps leading to the population of the fully relaxed first triplet state. The mechanism is summarized in the right side of Scheme 2. It should be remarked that the mechanism of the intersystem crossing process, including the intermediary states detected, and the overall time scales are very similar to what was observed for the parent compound 1-nitronaphthalene and should be considered a common type of behavior for many polycyclic nitroaromatic compounds with $\pi-\pi^*$ first singlet excited states that couple to the triplet manifold through an upper triplet state, which in turn relaxes in a slower time scale to the phosphorescent state (also of $\pi-\pi^*$ character). In fact, the ~10 ps time scale for relaxation into the lowest energy form of T_1 appears to be well in line with experiments where upper triplet states are populated by direct optical excitation of T_1.[47,48] Such experiments show times that range from 10 to 60 ps in several naphthalenic compounds for the recuperation of the relaxed T_1 population from internal conversion and vibrational relaxation within the triplet manifold.

Next, we make a more detailed analysis of the transient absorption data from NNA because in this compound we observed important changes in going from nonpolar to polar solvents. For the NNA/benzene system, we show representative single-wavelength traces and the respective detailed spectral evolution in Figure 9. The analysis of the transient absorption measurements for NNA/benzene does not include the time range where the solvent shows broad coherent spikes due to cross-phase modulation and benzene's polarizability. This reduces the actual time resolution of these experiments to near 1 ps. In the spectra of Figure 9, the long-lived species observed at $t > 11$ ps can be clearly identified as the phosphorescent state of this molecule from a comparison with previous measurements in the nanosecond time scale in the same solvent.[29] The signals

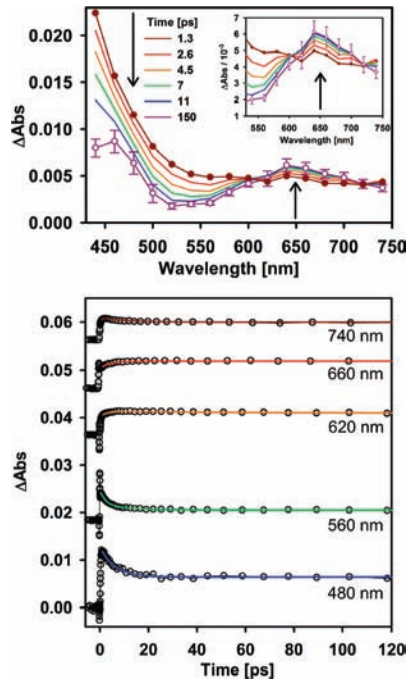

Figure 9. Transient spectral evolution (top), and single-wavelength transient absorption traces (bottom) for 4-nitro-1-naphthylamine in benzene. Solid lines correspond to fits to a multiexponential function plus a constant term. These experiments show a $t = 0$ modulation due to the solvent and the flow-cell. Fits only include the time range where this modulation is absent. For clarity, single-wavelength transients have been shifted in the ordinate axis.

preceding the appearance of this species must again be related to intersystem crossing and relaxation within the triplet manifold. The evolution of the signals was fitted to single- or double-exponential functions plus a constant term due to the persistence of the absorption from the T_1 state. The parameters are summarized in Table 2 and in the Supporting Information. They show a first component with time constants in the range from 1 to 10 ps for most wavelengths, and a few below 1 ps. The second exponential component has a slower value of at least ∼10 ps. Recalling that the up-conversion experiments showed that most of the fluorescence decays in a time scale of less than 150 fs (∼90%), we conclude that this part of the S_1 dynamics is unresolved in the transient absorption experiments (due to the cell and solvent artifacts near $t = 0$). Considering this, the spectral evolution of Figure 9 is mostly related to the relaxation already within the triplet manifold toward the T_1 state, including $T_n \rightarrow T_1$ internal conversion and vibrational relaxation. Similarly to both the parent compound 1-nitronaphthalene and MNN, strong absorbance is seen on the blue side of the spectrum at $t < 10$ ps, which is therefore assigned to the intermediary states in the triplet manifold that are transited as the population of the relaxed T_1 state accumulates. These signals ($\lambda < 600$ nm) decay as the broad band at 650 nm grows in intensity and the narrower band at 460 nm settles in the shape of the T_1 transient spectrum. Two nearly isosbestic points in the spectrum were observed at approximately 620 and 725 nm, where the absorption coefficients of the intermediaries and the final T_1 state have approximately the same value, confirming that the relaxed form of T_1 does accumulate from the $\lambda < 600$ nm absorbing intermediaries. This is detailed in the inset of Figure 9.

The transient absorption experiments for NNA in methanol display a completely different behavior, as shown in Figures 10−12. In this system, the transients at wavelengths that coincide with the center of the ground state's first band (420 and 440 nm) show a negative absorbance or "bleach", which recovers toward the baseline in two different time scales of ∼1 ps and from ∼8 ps (420 nm) to ∼19 ps (440 nm, see Table 2 and the Supporting Information). In this region, the trace then corresponds to a constant bleach signal of between 2% and 6% of the $t = 0$ value. At wavelengths from 460 to 620 nm, an instantaneous negative signal appears at the time origin, which is necessarily due to stimulated emission from S_1. From the initial negative value, the signal overshoots the baseline due to a first exponential term with negative amplitude and a time constant of a few hundred femtoseconds. Figure 11 shows a representative detail of this behavior at 520 nm together with a trace of the solvent-only scan (taken back to back), which verifies that in this experimental condition (methanol in a solution jet) the $t = 0$ modulations are practically absent. It should be noted that the time scale for the bleach or stimulated emission signals is indeed consistent with the results from the up-conversion experiments, which determined that more than 95% of the spontaneous fluorescence signal from the S_1 population decays within 200 fs (see Tables 1 and 2 and the Supporting Information).

After the subpicosecond evolution, a transient positive absorbance is observed in the visible region with an apparent peak at 460−520 nm and with minimal absorbance above 550 nm. This behavior is better illustrated in the time-resolved spectra of Figure 12. The 460−520 nm transient band reaches its maximum value at approximately 1 ps, and then decays in multiple time scales from ∼1 to ∼13.5 ps depending on the wavelength, leaving a very small amount of positive transient absorbance at long times (approximately only 1−2% of the maximum value but distinguishable from the baseline).

The instantaneous ground-state bleach followed by a biexponential recovery (420−440 nm), together with the appearance of a negative signal followed by a latter positive transitory signal at ∼1 ps, which subsequently collapses in the few picoseconds time scale (460−520 nm band), is a characteristic signature of the process of ultrafast recovery of the electronic ground state followed by vibrational cooling to reform the equilibrium S_0 state (see below). It should be emphasized that the NNA/methanol dynamics are vastly different from those in benzene and from those of 1-nitronaphthalene or MNN in any solvent (where the T_1 formation is unequivocally identified). Therefore, we can conclude that the solvent environment is playing the crucial role in changing the S_1 pathway in NNA.

Both the time scales and the general features of the NNA/methanol spectral evolution have been observed previously, for example, in several DNA bases,[49,50] azulene,[51] and *para*-nitroaniline.[41,42,52] In all of these systems, the $S_1 \rightarrow S_0$ internal conversion occurs via a conical intersection, which produces a population of vibrationally excited ground-state molecules after only a few molecular vibrations in the upper electronic surface. The instantaneous-negative transient absorption seen in our case indicates the bleach of the electronic ground state ($\lambda < 500$ nm) and/or a transient stimulated emission from S_1 (510−620 nm). The rapid conversion into the hot electronic ground state directly from S_1 implies a growth of absorption signals from the upper vibrational levels of S_0, which redounds in the appearance of a red-shifted spectrum in comparison with the fully relaxed S_0 state. This hot ground-state absorbance (460−520 nm band: $S_1 \leftarrow S_0$ (hot) transitions) then decays in the time scale of more than 10 ps in hydrogen-bonding solvents like methanol, where the S_0 (hot) relaxation has been described as multiexponetial due to stepwise energy flow to the first solvent shell, and then to the bulk.[52]

TABLE 2: Curve-Fitting Parameters for Selected Transient Absorption Traces of 4-Nitro-1-naphthylamine in Benzene and Methanol[a]

solvent	λ_{probe} [nm]	a_1	τ_1 [ps]	a_2	τ_2 [ps]	a_3	τ_3 [ps]	c
benzene[b,d]	480[c]	0.006	6.11			0.006		
benzene[b,e]	560[d]	0.003	2.54	0.001	13.40	0.002		
benzene[b,d]	660[c]	−0.002	3.87			0.006		
methanol[c,f]	420	−0.094	1.04	−0.099	7.93			−0.0119
methanol[c,f]	460	−0.115	0.34	0.061	4.51	−0.023	13.51	−0.0008
methanol[c,f]	520	−0.070	0.21	0.028	0.99			0.0014
methanol[c,f]	560	−0.022	0.11	0.008	0.81	−0.0004	10.29	0.0008
methanol[c,f]	640	0.005	0.62	0.0003	20.63			0.0005

[a] Data are described by single- or multiexponential functions plus a constant term, $\Delta\text{Abs}(t) = \sum_i a_i \cdot \exp(-t/\tau_i) + c$. Because of the longer time scale, fits for benzene experiments do not consider convolution with the instrument response function. For experiments in methanol, the instrument response function was between 220 and 410 fs, and the upper limit of the time scale was from 30 to 45 ps. All data have been scaled as shown in the following footnotes. [b] Transient absorption spectrum at 150 ps. [c] Short scans (see text). From the fitting procedure, the estimated error in parameters is as shown in the following footnotes. [d] Below 15%. [e] Between 20% and 50%. [f] Below 20%.

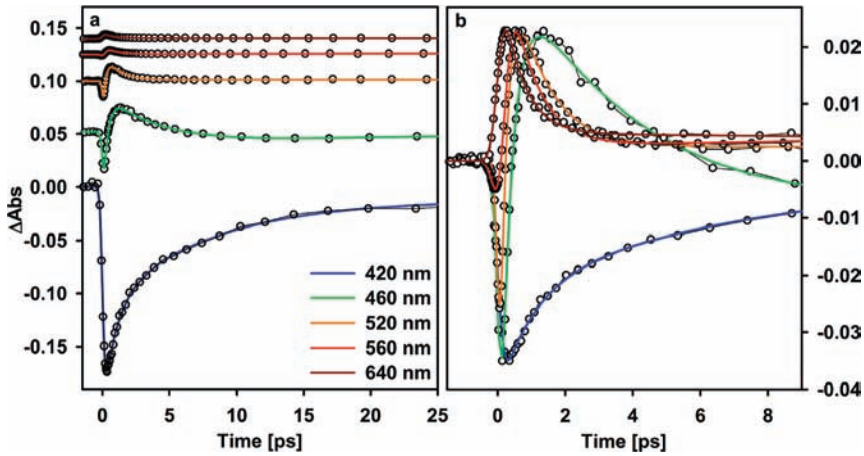

Figure 10. (a) Single-wavelength transient absorption traces for 4-nitro-1-naphthylamine in methanol. For clarity, single-wavelength transients have been shifted in the ordinate axis. (b) Traces have been normalized to the same value at the maximum amplitude. Solid lines correspond to fits to multiexponential functions plus a constant term. For these experiments, from the use of a free-flowing jet, it was possible to minimize the $t = 0$ solvent effect.

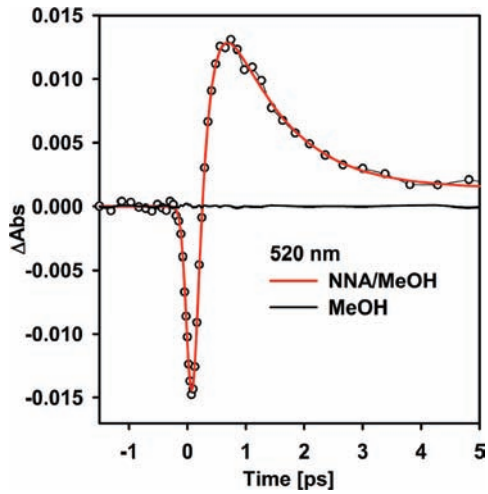

Figure 11. Detail of transient absorbance scan of 4-nitro-1-naphthylamine in methanol at 520 nm. The solid red line corresponds to a triple-exponential function plus a constant term. The solid black line indicates the results from a solvent-only scan under identical conditions showing the near absence of signal modulations due to the methanol in these experimental conditions using a free-flowing jet.

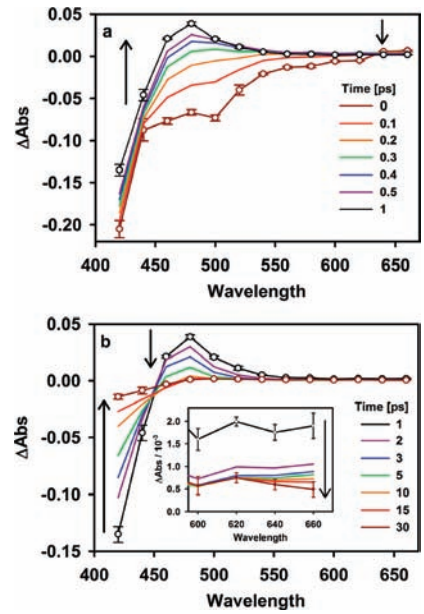

Figure 12. Transient spectra for 4-nitro-1-naphthylamine in methanol, from 0 to 1 ps (a) and from 1 to 30 ps (b).

Although these spectral signatures identify ultrafast internal conversion as the main decay channel for S_1 in NNA/methanol, which accounts for 94−98% of the originally excited population, the fact that the baseline for the 420−460 nm region does not fully recover, together with the remaining of a small positive absorbance at longer wavelengths, indicates that a small amount of the population of excited molecules does not recover to the ground state in this time scale due to the existence of an additional photochemical pathway with only a very small yield.

In fact, the absorbance after 30 ps is so near the baseline that a spectral identification of the species responsible for this signal was impossible. The residual transient absorption (at times after the S_0 recovery) undergoes a small amount of signal evolution occurring on larger time scales indicative of some type of relaxation and decay for the unidentified intermediary. This is documented in the Supporting Information where it can be seen that the absorbance from this long-lived species shows first a small amplitude rise of up to several tens of picoseconds and is followed by a slow decay in the time scale of a few nanoseconds. A probable assignment for this unidentified transitory species can be a small fraction of triplet states, which are formed in low yield due to the prevalence of the $S_1 \rightarrow S_0$ channel for NNA/methanol. The long time scans taken up to 700 ps of these small residual signals do show a decay in the 2−3 ns time scale. The disappearance in such time scales of this residual absorbance is consistent with the results from Capellos et al., who observed a lack of any transient absorbance after a 20 ns pulse for NNA/methanol.[29] This is also in agreement with Costela et al., who observed no transient species detectable with their resolution of 30 ns for NNA in ethyl acetate.[33]

Recalling the results of the excited-state calculations, for NNA the TD-DFT method indicates that, in going from methanol to benzene, the energy shifting for the first singlet excited state occurs in a different direction in comparison with the triplet states T_2 and T_3: while S_1 is stabilized, the two aforementioned triplets are slightly lifted in energy. Although the TD-DFT method is only approximate and we have used it primarily to characterize the vertical transition at the ground state, the results do suggest that the coupling between S_1 and particular vibroelectronic states in the triplet manifold of NNA will be changed simply in going from a nonpolar to a polar solvent. A similar argument has been proposed recently to explain the significant increase in the fluorescent state lifetime of 3-nitroperylene in comparison with 1-nitropyrene.[10] In that case, it was the increase in the size of the ring system (perylene vs pyrene) that could stabilize the S_1 state below a receiver triplet, thereby reducing the intersystem crossing channel. It should be stated, however, that besides this singlet−triplet decoupling argument, which should be operating also in NNA/methanol (due to the solvent-induced S_1 stabilization), our results show that in this system the ultrafast internal conversion to S_0 becomes highly dominant, this being the channel that drives the population out of the fluorescent state in the polar solvent. This is summarized on the left side of Scheme 2.

Conclusions

We have studied the photoinduced dynamics of two nitrated naphthalenes with an additional electron-donor substituent at the NO_2-*para* position. For the case of MNN, the dynamics are independent of the polarity of the solvent (cyclohexane vs methanol). This compound in methanol allowed a clear detection of all of the transient species involved in the ultrafast intersystem crossing, which is the main photoprocess for nitrated polyaromatics. Specifically, the evolution of MNN's first singlet excited state was observed for the first time through femtosecond fluorescence up-conversion, and the transit through intermediary upper triplet states into the relaxed phosphorescent triplet state was observed to occur on a longer time scale of tens of picoseconds by transient absorption spectroscopy. On the other hand, for the NNA molecule, we observed different decay paths for the spectroscopic first excited singlet state: In the nonpolar solvent (benzene), we observed dynamics similar to the case of MNN. However, in methanol, the transient absorption results for NNA indicate that the dominant channel corresponds to an ultrafast internal conversion to the electronic ground state followed by vibrational relaxation within S_0. Most importantly, we conclude that the additional stabilization of the S_1 state of NNA in methanol (which is not observed in MNN where the first electronic transition is solvent-insensitive) is responsible for the differences in the observed photoinduced dynamics. In particular, these results illustrate a key feature in many nitrated polyaromatics: the requirement of an energetic coincidence between the first singlet excited state of $\pi-\pi^*$ character, and upper intermediary states in the triplet manifold with some $n-\pi^*$ character. The TD-DFT results do suggest that the present systems allowed for a tuning of this energetic coincidence (solvatochromism in NNA), where, as the S_1 state is lowered in energy, the coupling with the "receiver" or intermediate triplet is reduced so that other trajectories in the potential energy surface of S_1 dominate the decay of this state.

Acknowledgment. We are thankful to Professor Ahmed H. Zewail and the California Institute of Technology for the donation of equipment used in this study. For financial support, we are thankful to Consejo Nacional de Ciencia y Tecnología (CONACyT, grant 79494), and to UNAM, PAPIIT grant 1N212907. The authors thank DGSCA-UNAM for computational resources.

Supporting Information Available: Tables of curve-fitting parameters for fluorescence up-conversion and transient absorption experiments on 1-methoxy-4-nitronaphthalene and 4-nitro-1-naphthylamine (including fitting parameters for long-time transient absorbance experiments for the last), figures of selected transient absorption experiments of 1-methoxy-4-nitronaphthalene in benzene and of 4-nitro-1-naphthylamine in methanol at long delay times, as well as graphical depictions of the frontier Kohn−Sham orbitals calculated at the TD-DFT level of theory, ground-state-optimized geometries, and single-excitation coefficients for the relevant electronic transitions. This material is available free of charge via the Internet at http://pubs.acs.org.

References and Notes

(1) Anderson, R. W., Jr.; Hochstrasser, R. M.; Lutz, H.; Scott, G. W. *Chem. Phys. Lett.* **1974**, *28*, 153.
(2) Capellos, C.; Porter, G. *J. Chem. Soc., Faraday Trans. 2* **1974**, *70*, 1159.
(3) Hamanoue, K.; Hirayama, S.; Nakayama, T.; Teranishi, H. *J. Phys. Chem.* **1980**, *84*, 2074.
(4) Hamanoue, K.; Hirayama, S.; Nakayama, T.; Teranishi, H. *Chem. Lett.* **1980**, 407.
(5) Heinz, B.; Schmierer, T.; Laimgruber, S.; Gilch, P. *J. Photochem. Photobiol., A* **2008**, *199*, 274.
(6) Hurley, R.; Testa, A. C. *J. Am. Chem. Soc.* **1968**, *90*, 1949.
(7) Rusakowicz, R.; Testa, A. C. *Spectrochim. Acta, Part A* **1971**, *27*, 787.
(8) Scheerer, R.; Henglein, A. *Ber. Bunsen-Ges. Phys. Chem.* **1977**, *81*, 1234.
(9) Wolfbeis, O. S.; Posch, W.; Guebitz, G.; Tritthart, P. *Anal. Chim. Acta* **1983**, *147*, 405.
(10) Mohammed, O. F.; Vauthey, E. *J. Phys. Chem. A* **2008**, *112*, 3823.
(11) Fournier, T.; Tavender, S. M.; Parker, A. W.; Scholes, G. D.; Phillips, D. *J. Phys. Chem. A* **1997**, *101*, 5320.
(12) Bunce, N. J.; Cater, S. R.; Scaiano, J. C.; Johnston, L. J. *J. Org. Chem.* **1987**, *52*, 4214.
(13) Görner, H. *J. Chem. Soc., Perkin Trans. 2* **2002**, 1778.
(14) Mikula, J. J.; Anderson, R. W.; Harris, L. E.; Stuebing, E. W. *J. Mol. Spectrosc.* **1972**, *42*, 350.
(15) Zugazagoitia, J. S.; Almora-Diaz, C. X.; Peon, J. *J. Phys. Chem. A* **2008**, *112*, 358.
(16) Hamanoue, K.; Nakayama, T.; Kajiwara, K.; Yamanaka, S.; Ushida, K. *J. Chem. Soc., Faraday Trans.* **1992**, *88*, 3145.
(17) Crespo-Hernández, C. E.; Burdzinski, G.; Arce, R. *J. Phys. Chem. A* **2008**, *112*, 6313.

(18) Jaffé, H. H.; Orchin, M. *Theory and Applications of Ultraviolet Spectroscopy*; John Wiley and Sons, Inc.: New York, 1962.

(19) Cvrèková, O.; Ciganek, M. *Polycyclic Aromat. Compd.* **2005**, *25*, 141.

(20) Fan, Z.; Chen, D.; Birla, P.; Kamens, R. M. *Atmos. Environ.* **1995**, *29*, 1171.

(21) Gerasimov, G. Y. *High Energy Chem.* **2004**, *38*, 161.

(22) Kamens, R. M.; Zhi-Hua, F.; Yao, Y.; Chen, D.; Chen, S.; Vartiainen, M. *Chemosphere* **1994**, *28*, 1623.

(23) Warner, S. D.; Farant, J.-P.; Butler, I. S. *Chemosphere* **2004**, *54*, 1207.

(24) Chapman, O. L.; Heckert, D. C.; Reasoner, J. W.; Thackaberry, S. P. *J. Am. Chem. Soc.* **1966**, *88*, 5550.

(25) Fukuhara, K.; Kurihara, M.; Miyata, N. *J. Am. Chem. Soc.* **2001**, *123*, 8662.

(26) Arce, R.; Pino, E. F.; Valle, C.; Ágreda, J. *J. Phys. Chem. A* **2008**, *112*, 10294.

(27) Hamanoue, K.; Amano, M.; Kimoto, M.; Kajiwara, Y.; Nakayama, T.; Teranishi, H. *J. Am. Chem. Soc.* **1984**, *106*, 5993.

(28) Hamanoue, K.; Nakayama, T.; Ushida, K.; Kajiwara, K.; Yamanaka, S. *J. Chem. Soc., Faraday Trans.* **1991**, *87*, 3365.

(29) Capellos, C.; Lang, F. *Int. J. Chem. Kinet.* **1977**, *9*, 409.

(30) Suzuki, T.; Nagae, O.; Kato, Y.; Nakagawa, H.; Fukuhara, K.; Miyata, N. *J. Am. Chem. Soc.* **2005**, *127*, 11720.

(31) Fukuhara, K.; Oikawa, S.; Hakoda, N.; Sakai, Y.; Hiraku, Y.; Shoda, T.; Saito, S.; Miyata, N.; Kawanishi, S.; Okuda, H. *Bioorg. Med. Chem.* **2007**, *15*, 3869.

(32) Costela, A.; García-Moreno, I.; García, O.; Sastre, R. *J. Photochem. Photobiol., A* **2000**, *131*, 133.

(33) Costela, A.; García-Moreno, I.; García, O.; Sastre, R. *Chem. Phys. Lett.* **2000**, *322*, 267.

(34) El-Sayed, M. A. *J. Chem. Phys.* **1963**, *38*, 2834.

(35) Zugazagoitia, J. S.; Collado-Fregoso, E.; Plaza-Medina, E. F.; Peon, J. *J. Phys. Chem. A* **2009**, *113*, 805.

(36) Morales-Cueto, R.; Esquivelzeta-Rabell, M.; Saucedo-Zugazagoitia, J.; Peon, J. *J. Phys. Chem. A* **2007**, *111*, 552.

(37) Peon, J.; Polshakov, D.; Kohler, B. *J. Am. Chem. Soc.* **2002**, *124*, 6428.

(38) Petrali, L.; Doria, F.; Verga, D.; Profumo, A.; Freccero, M. *J. Org. Chem.* **2009**, *74*, 1034.

(39) Adamo, C.; Scuseria, G. E.; Barone, V. *J. Chem. Phys.* **1999**, *111*, 2889.

(40) Frisch, M. J.; Trucks, G. W.; Schlegel, H. B.; Scuseria, G. E.; Robb, M. A.; Cheeseman, J. R.; Montgomery, J. A., Jr.; Vreven, T.; Kudin, K. N.; Burant, J. C.; Millam, J. M.; Iyengar, S. S.; Tomasi, J.; Barone, V.; Mennucci, B.; Cossi, M.; Scalmani, G.; Rega, N.; Petersson, G. A.; Nakatsuji, H.; Hada, M.; Ehara, M.; Toyota, K.; Fukuda, R.; Hasegawa, J.; Ishida, M.; Nakajima, T.; Honda, Y.; Kitao, O.; Nakai, H.; Klene, M.; Li, X.; Knox, J. E.; Hratchian, H. P.; Cross, J. B.; Bakken, V.; Adamo, C.; Jaramillo, J.; Gomperts, R.; Stratmann, R. E.; Yazyev, O.; Austin, A. J.; Cammi, R.; Pomelli, C.; Ochterski, J. W.; Ayala, P. Y.; Morokuma, K.; Voth, G. A.; Salvador, P.; Dannenberg, J. J.; Zakrzewski, V. G.; Dapprich, S.; Daniels, A. D.; Strain, M. C.; Farkas, O.; Malick, D. K.; Rabuck, A. D.; Raghavachari, K.; Foresman, J. B.; Ortiz, J. V.; Cui, Q.; Baboul, A. G.; Clifford, S.; Cioslowski, J.; Stefanov, B. B.; Liu, G.; Liashenko, A.; Piskorz, P.; Komaromi, I.; Martin, R. L.; Fox, D. J.; Keith, T.; Al-Laham, M. A.; Peng, C. Y.; Nanayakkara, A.; Challacombe, M.; Gill, P. M. W.; Johnson, B.; Chen, W.; Wong, M. W.; Gonzalez, C.; Pople, J. A. *Gaussian 03*, revision B.03; Gaussian, Inc.: Pittsburgh, PA, 2003.

(41) Thomsen, C. L.; Thøgersen, J.; Keiding, S. R. *J. Phys. Chem. A* **1998**, *102*, 1062.

(42) Kovalenko, S. A.; Schanz, R.; Farztdinov, V. M.; Hennig, H.; Ernsting, N. P. *Chem. Phys. Lett.* **2000**, *323*, 312.

(43) Mataga, N.; Shibata, Y.; Chosrowjan, H.; Yoshida, N.; Osuka, A. *J. Phys. Chem. B* **2000**, *104*, 4001.

(44) Peon, J.; Zewail, A. H. *Chem. Phys. Lett.* **2001**, *348*, 255.

(45) Swayambunathan, V.; Lim, E. C. *J. Phys. Chem.* **1985**, *89*, 3960.

(46) Swayambunathan, V.; Lim, E. C. *J. Phys. Chem.* **1987**, *91*, 6359.

(47) Sakamoto, M.; Cai, X.; Hara, M.; Fujitsuka, M.; Majima, T. *J. Am. Chem. Soc.* **2004**, *126*, 9709.

(48) Sakamoto, M.; Cai, X.; Hara, M.; Fujitsuka, M.; Majima, T. *J. Phys. Chem. A* **2005**, *109*, 4657.

(49) Pecourt, J. M. L.; Peon, J.; Kohler, B. *J. Am. Chem. Soc.* **2000**, *122*, 9348.

(50) Pecourt, J. M. L.; Peon, J.; Kohler, B. *J. Am. Chem. Soc.* **2001**, *123*, 10370.

(51) Sukowski, U.; Seilmeier, A.; Elsaesser, T.; Fischer, S. F. *J. Chem. Phys.* **1990**, *93*, 4094.

(52) Kovalenko, S. A.; Schanz, R.; Hennig, H.; Ernsting, N. P. *J. Chem. Phys.* **2001**, *115*, 3256.

JP905379Y